Article

Turning Waste into Wealth: Sustainable Amorphous Silica from Moroccan Oil Shale Ash

Anas Krime [1,2,3,*], Sanaâ Saoiabi [1], Mouhaydine Tlemcani [2,3], Ahmed Saoiabi [1], Elisabete P. Carreiro [4,*] and Manuela Ribeiro Carrott [4,5]

1   Applied Materials Chemistry Laboratory, Department of Chemistry, Faculty of Sciences, Mohammed V University in Rabat, Avenue Ibn Batouta, Rabat B.P.1014, Morocco; sanaa.saoiabi@yahoo.com (S.S.); saoiabi.ahmed@yahoo.com (A.S.)
2   Instrumentation and Control Laboratory-LAICA, Center for Sci-Tech Research in Earth System and Energy, CREATE, University of Evora, 7000-671 Evora, Portugal; tlem@uevora.pt
3   Laboratory of Water, Center for Sci-Tech Research in Earth System and Energy, CREATE, University of Evora, 7000-671 Evora, Portugal
4   Associate Laboratory for Green Chemistry—LAQV-REQUIMTE, IIFA, University of Evora, 7000-671 Evora, Portugal; manrc@uevora.pt
5   Department of Chemistry and Biochemistry, School of Sciences and Technology, University of Evora, 7000-671 Evora, Portugal
*   Correspondence: anas.krime@um5r.ac.ma (A.K.); betepc@uevora.pt (E.P.C.)

Abstract

Moroccan oil shale ash (MOSA) represents an underutilized industrial by-product, particularly in the Rif region, where its high mineral content has often led to its neglect in value-added applications. This study highlights the successful conversion of MOSA into amorphous mesoporous silica (AS-Si) using a sol–gel process assisted by polyethylene glycol (PEG-6000) as a soft template. The resulting AS-Si material was extensively characterized to confirm its potential for environmental remediation. FTIR analysis revealed characteristic vibrational bands corresponding to Si–OH and Si–O–Si bonds, while XRD confirmed its amorphous nature with a broad diffraction peak at $2\theta \approx 22.5°$. SEM imaging revealed a highly porous, sponge-like morphology composed of aggregated nanoscale particles, consistent with the nitrogen adsorption–desorption isotherm. The material exhibited a specific surface area of 68 m^2/g, a maximum in the pore size distribution at a pore diameter of 2.4 nm, and a cumulative pore volume of 0.11 cm^3/g for pores up to 78 nm. DLS analysis indicated an average hydrodynamic diameter of 779 nm with moderate polydispersity (PDI = 0.48), while a zeta potential of −34.10 mV confirmed good colloidal stability. Furthermore, thermogravimetric analysis (TGA) and DSC suggested the thermal stability of our amorphous silica. The adsorption performance of AS-Si was evaluated using methylene blue (MB) and ciprofloxacin (Cipro) as model pollutants. Kinetic data were best fitted by the pseudo-second-order model, while isotherm studies favored the Langmuir model, suggesting monolayer adsorption. AS-Si could be used four times for the removal of MB and Cipro. These results collectively demonstrate that AS-Si is a promising, low-cost, and sustainable adsorbent derived from Moroccan oil shale ash for the effective removal of organic contaminants from aqueous media.

Keywords: Moroccan oil shale ash; neglected; amorphous silica; methylene blue; ciprofloxacin; aqueous media

1. Introduction

Oil shale falls under the category of unconventional oils that are considered as a crucial alternative resource of the production of energy at low cost. It is known that the main use of oil shale is to produce petroleum oil and gas due its specific composition and structure [1]. Indeed, the conversion of oil shale into fuel and chemical products can be performed by gasification, during the course of which the organic matter of shale is converted into a mixture of carbon oxides and hydrogen, or it can undergo by pyrolysis to have gaseous, liquid, and solid products [2].

Morocco has the sixth-largest world oil shale reserve, mainly in Timahdit and Tarfaya deposits [3]. Since 1980, the National Office of Mines and Hydrocarbons (ONHYM) has improved an advanced technology to extract oil from this abundant resource, but they had drawbacks, including a significant by-product named oil shale ash (OSA) and economic damage [4]. Consequently, the urgency of implementing a proper ash handling strategy has become the focus of research.

Recently, several studies have proven the usefulness of this residue (OSA) in various scientific and industrial domains such as cement ceramics, construction and alkali-activated materials, and environmental remediation owing to its physico-chemical composition [5–7]. The large mineral component is silicon dioxide (SiO_2), so oil shale ash offers a cheaper and sustainable silica source for producing high-grade silica, such as silica aerogels [8], compared to costly commercial products such as tetraethoxysilane (TEOS) and tetramethoxysilane (TMOS) [9].

Silica, being one of the most prevalent compounds found on Earth and in the lithosphere, holds a key position as an indispensable and efficient inorganic adsorbent used to remove organic pollutants from water and make it potable, especially in developing countries [10,11].

Antibiotics and dyes are the most common contaminants discharged into water as result of the widest spread of industrialization and population growth [12]. These organic pollutants can excrete into human bodies, plants, wastewater, and animals leading to serious damage to human health and well-being, photosynthesis inhibition, antibiotic resistance, and an unbalanced environment [13]. Thus, it is important to promote the immediate employment of advanced technologies such as photocatalysis and adsorption to remove these organic pollutants [14].

This study intends to recycle MOSA by producing amorphous silica. The by-product MOSA was successfully used to produce silica using a sol–gel process and used as an efficient adsorbent for the removal of organic contaminants (methylene blue and ciprofloxacin) from aqueous solution. The labeled silica AS-Si was characterized using analytical techniques including scanning electron microscopy with energy-dispersive X-ray (SEM/EDX), Fourier transform infrared–attenuated total reflectance (FTIR-ATR) spectroscopy, X-ray diffraction (XRD), thermal analysis (TGA and DSC), nitrogen adsorption at 77 K, and dynamic light scattering (DLS) analysis. To understand the mechanism of adsorption from solution, the kinetic and equilibrium data were analyzed using the non-linear pseudo-first-order, pseudo-second-order, Langmuir, and Freundlich models.

2. Results and Discussion

2.1. Characterization of the Material

2.1.1. Brunauer–Emmett–Teller (BET) and NLDFT Analyses

Figure 1 shows both the nitrogen physisorption isotherm at 77 K for silica (AS-Si) and the estimated distribution of pore size using NLDFT analysis. It is observed that although the adsorption branch resembles a type II isotherm of the IUPAC classification [15,16], the isotherm presents genuine hysteresis extending to below 0.4 p^o, which may suggest a

non-rigid porous structure [15,16]. The analysis using the BET method indicates a specific surface area of 68 m^2 g^{-1}, which is reasonable, although not as high as those of silica aerogels produced from oil shale ash [8]. The results of the NLDFT pore size distribution confirm the mesoporous structure of AS-Si (2<D_P>50 nm), with a maximum at 2.4 nm while the total cumulative pore volume for pores up to 78 nm attained is 0.11 cm^3 g^{-1}.
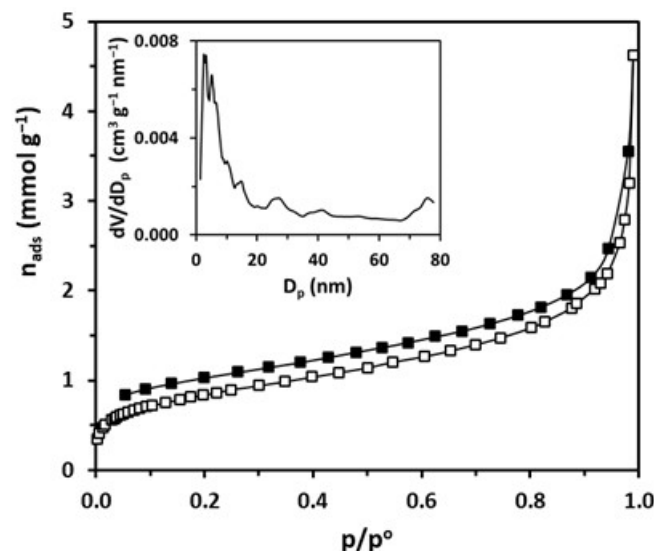

Figure 1. Nitrogen adsorption–desorption isotherm determined at 77 K on silica AS-Si (open symbols—adsorption, filled symbols—desorption). The inset shows the NLDFT pore size distribution.

2.1.2. Fourier Transform Infrared Spectroscopy (FTIR)

The functional groups of AS-Si, illustrated in Figure 2, were obtained using FTIR-ATR analysis. The absorption band region at 3445 and 1630 cm^{-1} indicated the presence of the O-H stretching and bending modes, which are characteristic of hydroxyl groups and water molecules [17]. In addition, the absorption bands located at 1120, 920, 800, and 452 cm^{-1} are characteristics of SiO$_2$ [18]. The asymmetric vibration of siloxane (Si-O-Si) and the stretching vibration of silanol (Si-OH) give rise to a wide spectral band at 1120 cm^{-1} and 920 cm^{-1}, respectively. Furthermore, the symmetry vibration linkages within the siloxane structure (Si-O-Si) were observed at 800 and 452 cm^{-1} [19].
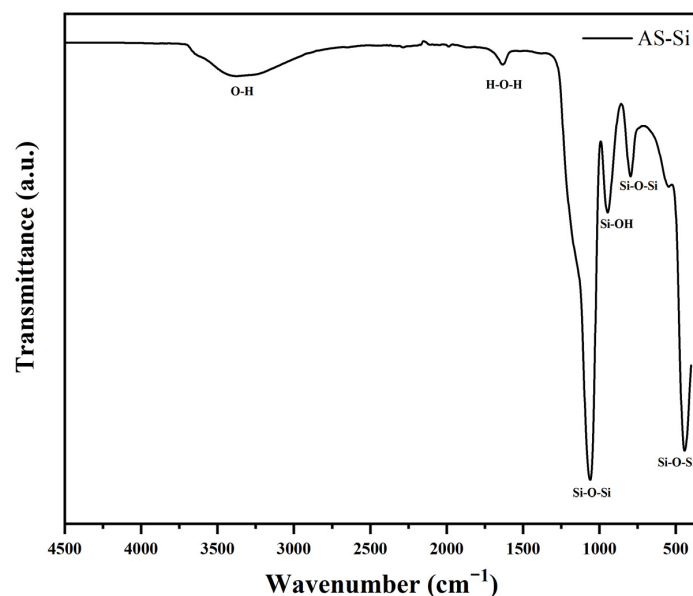

Figure 2. FTIR spectra of the studied silica AS-Si.

2.1.3. Scanning Electron Microscopy (SEM)

Figure 3 depicts the micrograph of the silica AS-Si that shows non-uniform shapes and loosely arranged clusters of particles (resembling a sponge) with a highly porous structure [20], which renders this silica well-suited as an efficient adsorbent. Furthermore, the EDX analysis ascertained the main silica phase with an elemental composition of 54.10 wt% and 33.45 wt% of oxygen and silicon, respectively. The weight percentage of carbon (10.05 wt%) presented in the table of Figure 3 is probably related to residual PEG-6000 and possibly to the formation of surface carbonates, which are obtained from the reaction between the residue of hydroxide sodium used during the process and atmospheric CO_2 during storage [21,22]. In addition, the sodium observed in trace amounts (2.38 wt%) originates from the alkaline step during the process. Additionally, the atomic ratio of silicon to oxygen (1:2.8) corresponds to the stoichiometric ratio of natural silica as reported in our previous work [23], which confirms the successful production of amorphous silica from the MOSA [20,24].
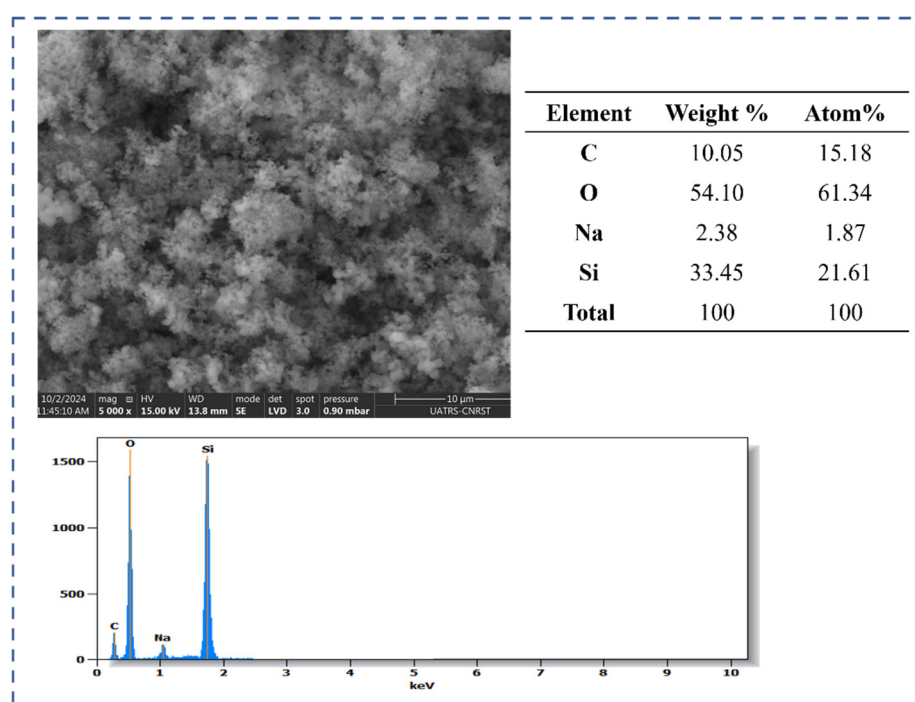

Element	Weight %	Atom%
C	10.05	15.18
O	54.10	61.34
Na	2.38	1.87
Si	33.45	21.61
Total	100	100

Figure 3. SEM micrograph and EDX analysis of AS-Si.

2.1.4. Thermal Analysis (TGA and DSC)

The temperature is an important factor that affects the morphology of the silica [25]. In order to study the thermal behavior of AS-Si, two widely used methods, including thermogravimetric analysis (TGA) and differential scanning calorimetry (DSC), were applied to investigate the thermal properties from room temperature to 900 °C (Figure 4).

The curve of TGA in Figure 4a presented a total weight loss of approximately 16.5% observed in the three phases. The evaporation of the physically adsorbed water is responsible for the first weight loss below 130 °C, while the second one, which is a negligible weight loss ranging from 130 to 350 °C, may be due to the presence of polyethylene glycol (PEG-6000) residue, which was used during the process. When the temperature exceeds 350 °C, a slight and continuous weight loss can be attributed to dehydroxylation of the silica surface (silanol groups). Along with the findings of the TGA analysis, several endothermic and exothermic transitions occurred in the DSC graph (Figure 4b), particularly near 119 °C and 855 °C, respectively. The first endothermic peak at 119 °C is associated with dehydration from the AS-Si surface, while the second one observed at 813 °C and the exothermic shift

at 855 °C may indicate the incipient crystallization of the AS-Si matrix, making it suitable for advanced applications under high temperatures [25–27].
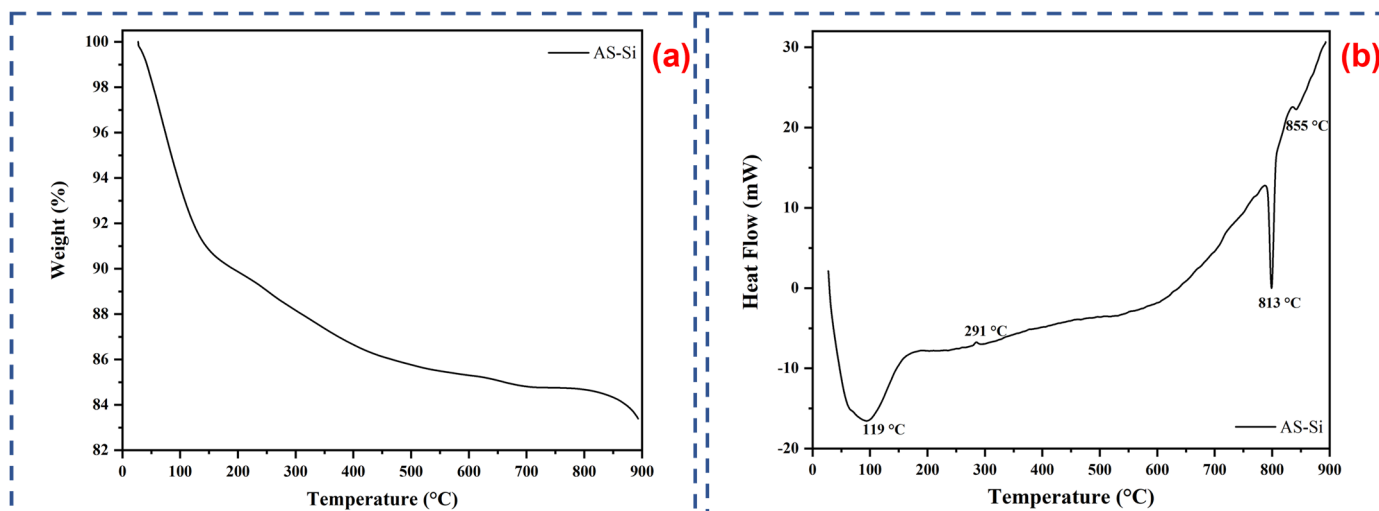

Figure 4. TGA (**a**) and DSC (**b**) curves of silica AS-Si.

2.1.5. X-Ray Diffraction Analysis (XRD)

Figure 5 depicts the pattern determined using X-ray diffraction (XRD) of the synthesized silica from MOSA. The diffraction pattern of silica exhibits a broad peak approximately centered around 22º (2θ), as in [28], indicating the amorphous state of the AS-Si. The absence of sharp diffraction peaks confirms the absence of any crystalline form of silica or other crystalline impurities.
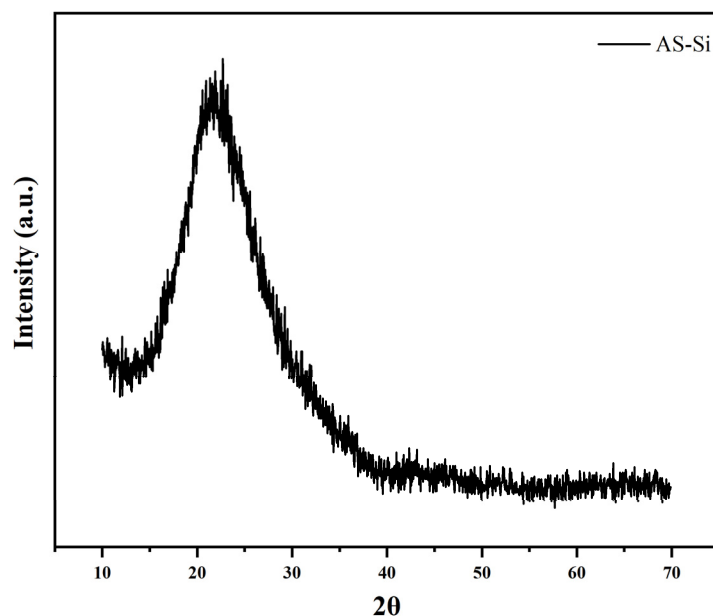

Figure 5. X-ray diffraction pattern of AS-Si.

2.1.6. Hydrodynamic Diameter, Polydispersity Index (PDI), and Zeta Potential

DLS analysis of the AS-Si sample in water as dispersion medium revealed a Z-average hydrodynamic diameter of 779.55 $\pm$ 9.12 nm, suggesting aggregates in the submicron range in the suspension, which is confirmed by the porous network morphology in the SEM image. Moreover, the PDI of 0.48 $\pm$ 0.09 exhibits a mid-range polydispersity (typically <0.7) with a broad particle size distribution due to the heterogeneous properties of the

oil shale ash as a source. The zeta potential of AS-Si reveals a good colloidal stability due to the negative surface charge inferred from the zeta potential of -34.10 ± 0.28 mV (typically >-30 mV). These findings align with the measurements reported for silica by the research groups of Gubala and Kumarathasan, with a zeta potential of -34.4 mV, PDI of approximately 0.374, and hydrodynamic diameters ranging from 657.4 to 1128.0 nm [29,30].

2.2. Tests of Adsorption of Methylene Blue and Ciprofloxacin onto AS-Si
2.2.1. Kinetic Models

Time is one of the most important factors impacting adsorption [31]. To describe how the adsorbent can behave over time, the two most common kinetics models, pseudo-first-order and pseudo-second-order models, were implemented to fit the experimental data. The calculated parameters of the non-linear plots were determined with a range of 0 to 300 min (using 12 and 13 experimental data points for ciprofloxacin and MB, respectively), an adsorbent mass of 0.2 g and a natural pH of both organic species (methylene blue and ciprofloxacin).

Figure 6 revealed a rapid adsorption during the first 20 min for both methylene blue (MB) and ciprofloxacin (Cipro). The adsorption continued then until the plateau was reached in 90 min and 180 min for MB and Cipro, respectively, with a percentage removal of 98% for MB and 81% for Cipro.
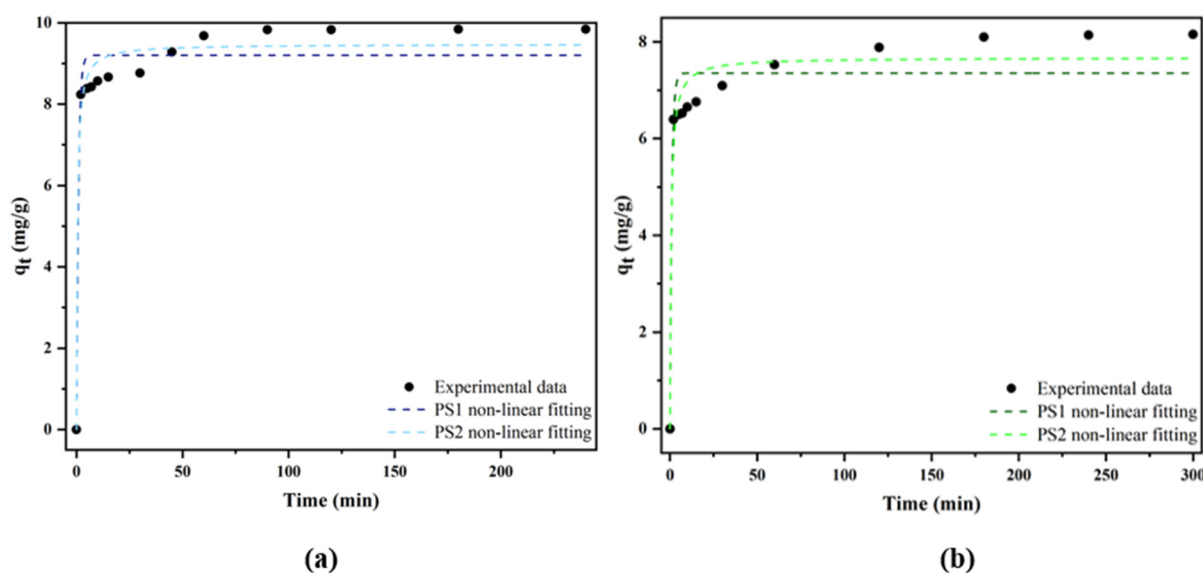

Figure 6. The non-linear fitting of pseudo-first (PS1) and second-order (PS2) models of methylene blue (**a**) and ciprofloxacin (**b**) onto AS-Si.

Based on the parameters obtained from the non-linear fitting, it was noticed that the pseudo-second-order model describes the adsorption of both organic pollutants (methylene blue and ciprofloxacin), as determined by the high determination coefficients ($R^2 = 0.9714$ for MB and 0.9530 for Cipro) and low values of SSE and RMSE (Table 1).

The adsorption most likely occurs through specific interactions, aligning with the characterization of AS-Si, notably of the mesoporous structure and the strong negative charge (zeta potential of -34.10 mV) of the sample. The pore size distribution (inset of Figure 1) indicates that the pores of AS-Si are wide enough for both organic pollutants to access. The negative charge, inferred from the negative zeta potential, is consistent with predictions based on the pH value at the point of zero charge (pH_{PZC}) of silica, which is around 2 [32]. In the present work, the pH is 6.5, which is above the pH_{PZC}, so the adsorbent surface is negatively charged under these conditions, thereby promoting

association through electrostatic attraction with methylene blue and ciprofloxacin, although hydrogen bonding may also be involved in the adsorption process. In the case of MB, which has pKa values of 3.63 and 11.56 [33], the predominant ionic species at pH 6.5 is the cationic form, MB^{2+} [33], which can interact with the negatively charged silica surface through electrostatic attraction, as illustrated in Figure 7a. For Cipro, with pKa values of 5.9 and 8.9 [34], the molecule exists predominantly in its zwitterionic form ($Cipro^0$) at pH 6.5 [34], which can interact electrostatically with the negatively charged adsorbent via the positively charged group [34], as illustrated in Figure 7b. Nevertheless, it is possible that hydrogen bonding may also occur as exemplified in Figure 7. The outcomes of this study are in agreement with several studies found in the literature on the silica-based materials [35].

Table 1. Kinetic parameters of non-linear models fitted for removal of methylene blue and ciprofloxacin.

		AS-Si	
		MB	**Cipro**
Pseudo-first-order model	q_e(Cal) (mg g^{-1})	9.2031 ± 0.1821	7.3544 ± 0.2122
	K_1 (min^{-1})	1.082 ± 0.2943	0.9508 ± 0.3127
	R^2	0.9473	0.9103
	SSE	3.9355	4.3558
	RMSE	1.9838	2.0970
Pseudo-second-order model	q_e(Cal) (mg g^{-1})	9.4750 ± 0.1615	7.6750 ± 0.1879
	K_2 (g mg^{-1} min^{-1})	0.2246 ± 0.694	0.1925 ± 0.0640
	R^2	0.9714	0.9530
	SSE	2.1322	2.2822
	RMSE	1.4602	1.5106

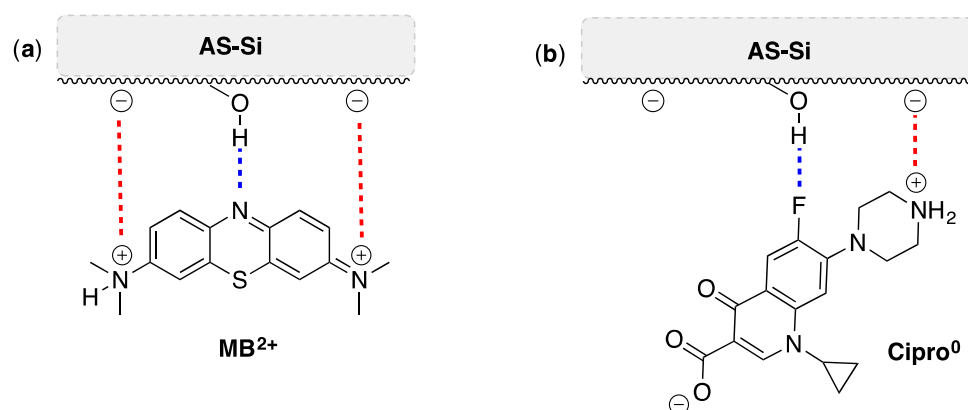Values are expressed as mean $\pm$ standard error (SE).

Figure 7. Proposed interactions between the AS-Si adsorbent surface and MB^{2+} (**a**) and $Cipro^0$ (**b**) in aqueous media.

2.2.2. Isotherms

The concentration of the pollutant significantly affects the uptake [36]. From this viewpoint, the equilibrium uptake of both contaminants (methylene blue and ciprofloxacin) onto amorphous silica (AS-Si) was fitted using the non-linear models of Langmuir and Freundlich (using 10 experimental data points) under the same previous conditions of mass and pH.

The results obtained from Figure 8 show that the adsorption increased with the concentration and continued until it reached the saturation for two organic pollutants (methylene blue and ciprofloxacin). Furthermore, the Langmuir isotherm more accurately described the equilibrium data for methylene blue and ciprofloxacin with $R^2 = 0.8278$ and $R^2 = 0.9506$, respectively (Table 2). Thus, we presumed a monolayer adsorption due to the properties (moderate surface area, negative zeta potential, and mesoporous structure) of AS-Si. It is also important to note that q_m values are comparable to the experimental adsorption capacities (q_e) for the two organic pollutants investigated (MB and Cipro).
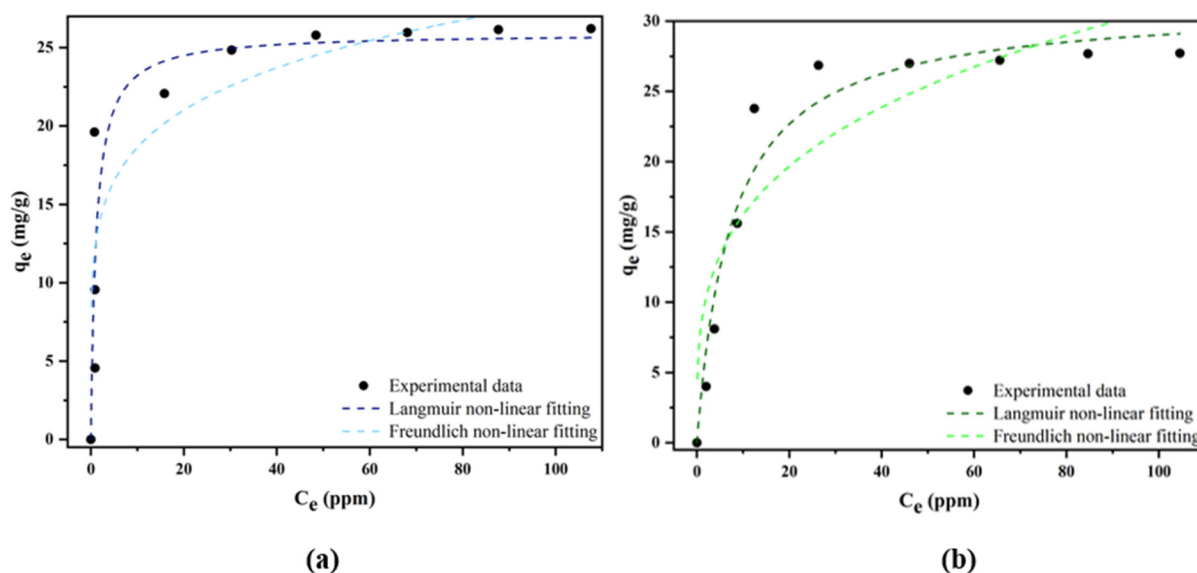

(a)   **(b)**

Figure 8. The non-linear fitting of Langmuir and Freundlich models of methylene blue (**a**) and ciprofloxacin (**b**) onto AS-Si.

Table 2. Calculated parameters of non-linear isotherms fitted for removal of methylene blue and ciprofloxacin.

		AS-Si	
		MB	**Cipro**
Langmuir	q_m **(mg g^{-1})**	25.9118 ± 1.8458	31.1804 ± 1.6416
	K_L **(L mg^{-1})**	0.28654 ± 0.3569	0.1333 ± 0.0300
	R^2	0.8278	0.9506
	SSE	137.3734	42.3328
	RMSE	11.7206	6.5063
Freundlich	K_F **((mg g^{-1}) ((L mg^{-1})$^{1/n}$))**	12.4672 ± 2.3616	8.5223 ± 2.3527
	1/n	0.1742 ± 0.0490	0.2792 ± 0.704
	R^2	0.6916	0.7474
	SSE	139.9143	152.4881
	RMSE	11.8285	12.3486

Values are expressed as mean $\pm$ standard error (SE).

Our analysis findings indicate consistency with the existing literature on amorphous silica, which demonstrated that the Langmuir model fitted well the uptake removal of ciprofloxacin and methylene blue [37,38].

2.3. Comparative Study

Table 3 presents the comparative study conducted to highlight the uptake capacity of this mesoporous silica (AS-Si) compared to other waste-based materials. The results obtained demonstrate that our amorphous silica exhibits an efficient removal capacity for both organic pollutants (methylene blue and ciprofloxacin), positioning AS-Si as a superior or competitive adsorbent for the treatment of dyes and antibiotics from wastewater.

Table 3. Comparative analysis of the adsorption capacity of AS-Si for methylene blue (MB) and ciprofloxacin (Cipro) against reference data from waste-based materials reported in the literature.

Adsorbent Material	Process	Pollutant	Initial Concentration (ppm)	Adsorbent Dose	Contact Time (min)	Adsorbed Quantity (mg/g)	Reference
Fly ash	Pretreated with hot distilled water and dried at 105 °C	MB	100	600 mg	120	5.7169	[39]
Neem leaves	Pretreatment including: washing with distilled water, dried in an oven at 333–343 K, crushing	MB	40	200 mg	60	8.76	[40]
Raw RHA	No pretreatment	MB	10	500 mg	180	3.01	[41]
Treated RHA	Mechanochemical treatment	MB	10	500 mg	180	5.02	[41]
AS-Si	Sol-gel	MB	20	200 mg	90	9.82	This work
Modified fly ash	Modification trough microwave power	Cipro	100	100 mg	120	11.76	[42]
Zeolite-modified nano-flakes	Modification trough different steps: alkaline treatment with NaOH, acid and re-precipitation using HCL, Filtration, neutralization with distilled water and dried at 280 °C using an electro-thermostatic blast oven (YLD-2000)	Cipro	20	100 mg	120	7.67	[43]
AS-Si	Sol–gel	Cipro	20	200 mg	180	8.10	This work

2.4. Regeneration Study

The reusability of the adsorbent during the adsorption process is an important factor for practical applications. The stability and repeatability of the amorphous silica were tested using the same experimental conditions for four cycles, where a mixture solution (90/10) of ethanol and distilled water was used for methylene blue [44], while a mixture of ethanol and NaOH (50:50) was investigated for ciprofloxacin [45]. Figure 9 revealed a percentage removal after 4 cycles of up to 90% and 72% for methylene blue and ciprofloxacin, respectively, consistent with similar results of silica derived from bio-sources in the literature [46]. Thus, this confirms the capability of AS-Si to be reutilized, highlighting its potential for both economic savings and environmental sustainability.
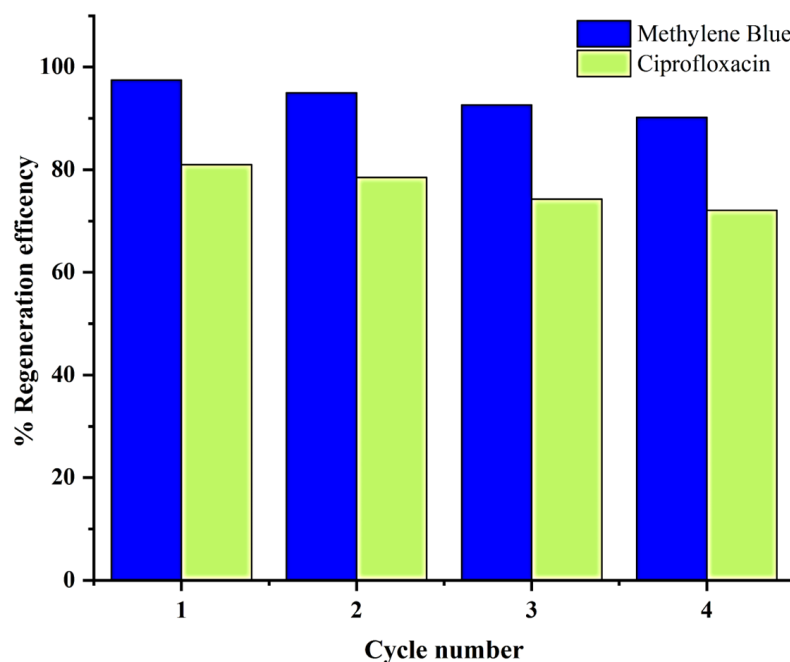
Figure 9. The regeneration efficiency of methylene blue and ciprofloxacin onto AS-Si.

2.5. FTIR and XRD After Adsorption

The AS-Si materials after the adsorption of MB and Cipro were analyzed using FTIR-ATR spectroscopy and XRD and compared with the AS-Si adsorbent prior to the adsorption process, as shown in the spectra and diffractograms in Figures 10 and 11, respectively. By comparing the FTIR spectra before and after pollutants adsorption, it is evident that the adsorbent retains the same profile and characteristic bands, clearly demonstrating its stability and robustness during these tests. However, a slight decrease in the intensity of the main absorption bands, O-H, Si-O-Si and Si-OH, was observed in both cases, which could be attributed to the interactions established between the adsorbent and the MB and Cipro species adsorbed.
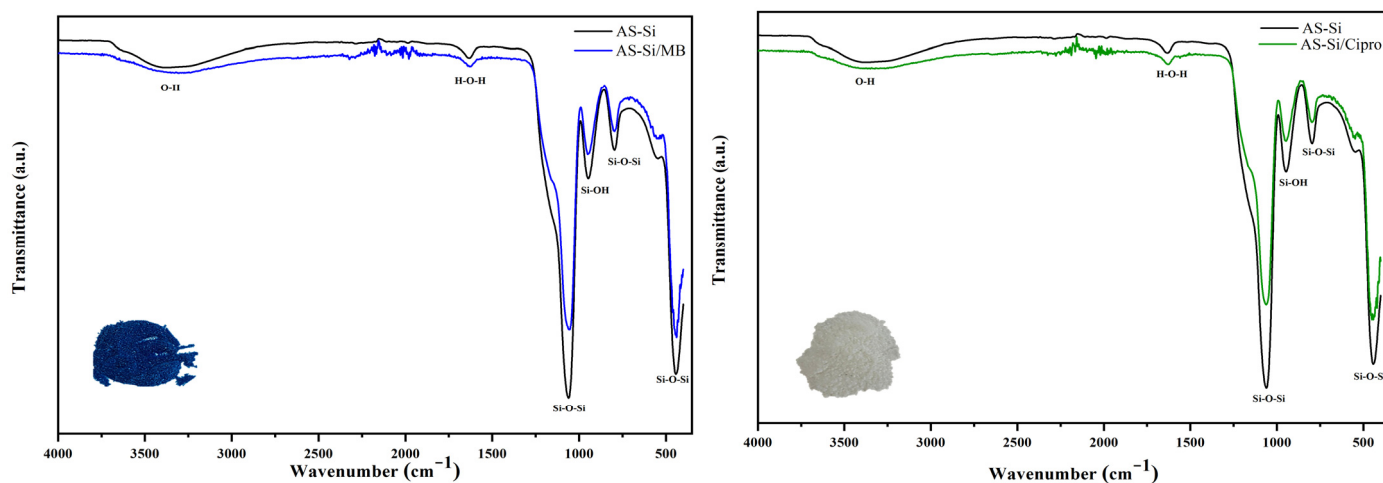

Figure 10. The FTIR analysis before (AS-Si) and after adsorption of methylene blue (AS-Si/MB) and ciprofloxacin (AS-Si/Cipro) onto AS-Si.
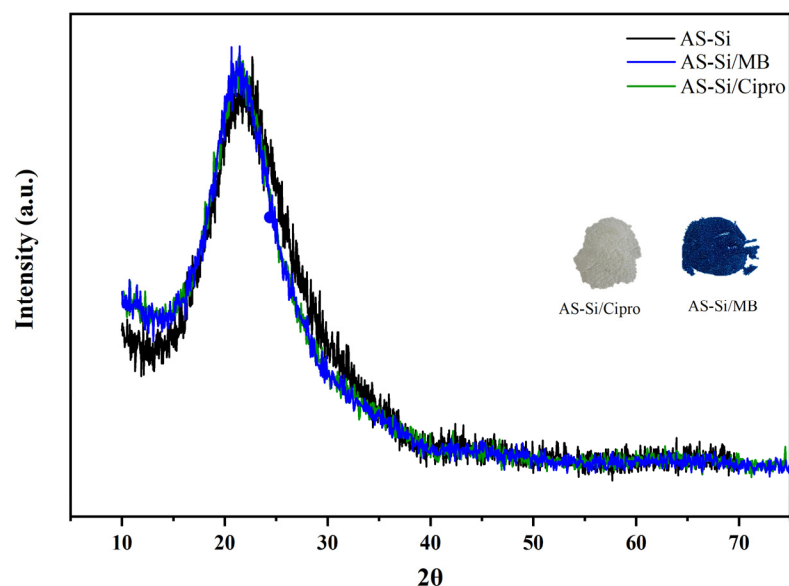
Figure 11. The XRD patterns before (AS-Si) and after adsorption of methylene blue (AS-Si/MB) and ciprofloxacin (AS-Si/Cipro) onto AS-Si.

Regarding the XRD patterns before and after the adsorption of Cipro and MB, a broad peak centered around 22.5°, characteristic of amorphous silica, was observed in all samples. The results showed no significant changes in the XRD patterns after pollutant adsorption, confirming the structural stability of the amorphous AS-Si throughout the process.

3. Materials and Methods

3.1. Materials

The source of silica was collected from the Rif deposit with chemical components of 71.20% SiO_2, 3.90% alumina (Al_2O_3), 2.82% iron oxide (Fe_2O_3), and small amount less than 0.5% of magnesium oxide (MgO), titanium dioxide (TiO_2), phosphorus pentoxide (P_2O_5), and calcium oxide (CaO).

All chemical reagents utilized in this work were of analytical grade and implemented without further purification. Sodium hydroxide in pellets form (97% purity), sulfuric acid (98% purity), hydrochloride acid (37% purity), ethanol (99.8% purity), and polyethylene glycol-6000 ($\geq$99% purity) were purchased from Sigma-Aldrich, while organic pollutants used in the adsorption experiments including methylene blue ($\geq$82% dye content) and ciprofloxacin ($\geq$98% purity) were from VWR Chemicals.

3.2. Sol–Gel Process

The oil shale ash was pretreated through a sequence of procedures [47], including grinding, an acid washing step with sulfuric acid (3.7 mol/L), filtration, neutralization, and sieving to obtain particles of <0.2 mm. Furthermore, 25 g of the treated sample was then added to 200 mL of sodium hydroxide solution with a 10.0 mol/L concentration and stirred magnetically at a controlled temperature of 95 °C for 4 h.

The sodium silicate obtained was filtered, washed with a trace amount of boiled distilled water, and cooled to room temperature. Then, the suspension was carefully dispersed into a solution of 0.0154 mol/L polyethylene glycol-6000 before it was sonicated at 45 °C. Additionally, 0.5 mol/L sulfuric acid was added slowly to the mixture until it reached pH 4 to form the gel through hydrolysis and condensation, which was filtered, washed several times, and dried overnight at 110 °C. Finally, it was calcined at 550 °C for 2 h to remove the PEG-6000 used as a surfactant. The average yield from the treated oil shale ash across three experiments is 80%.

3.3. Adsorption from Solution Experiments

Adsorption experiments were carried out through the preparation of two different stock solutions for each organic species (methylene blue and ciprofloxacin). The concentration of each resulting suspension during the adsorption test was determined using an UV–Vis spectrophotometer (UV-6300 PC) at a maximum absorbance wavelength of 664 and 277 nm for methylene blue and ciprofloxacin, respectively. The adsorbent mass used in all experiments was 0.2 g based on the results of preliminary tests shown in Figure S1 of the Supplementary Materials.

The quantity adsorbed was calculated using Equation (2) as follows [48]:

$$q_t = \frac{(C_0 - C_e)}{m}V \tag{1}$$

where the initial and equilibrium concentrations denoted C_0 and C_e, respectively, were expressed in mg/L. The solution volume (V) is in L, and the adsorbent mass (m) is in g.

3.4. Models for Isotherm and Kinetic Studies

The non-linear forms of the pseudo-first-order (3), pseudo-second-order (4), Langmuir (5), and Freundlich (6) models were fitted employing the software origin lab (2018 SR1). The equations of the experimental data are presented as follows:

- Pseudo-first-order kinetic non-linear model [49]:

$$q_t = q_e\left(1 - e^{-K_1 t}\right) \tag{2}$$

- Pseudo-second-order kinetic non-linear form [50]:

$$q_t = \frac{K_2 q_e^2 t}{1 + K_2 t q_e} \tag{3}$$

Here, q_t and q_e are the adsorption capacity of pollutants at time t and equilibrium, respectively. In addition, K_1 (min^{-1}) and K_2 (g mg^{-1} min^{-1}) define the admissible constants of the kinetic rate.

- Langmuir isotherm non-linear form [51]:

$$q_e = \frac{q_m K_L C_e}{1 + K_L C_e} \tag{4}$$

- -Freundlich isotherm non-linear shape [52]:

$$q_e = K_F C_e^{\frac{1}{n}} \tag{5}$$

Here, q_m (mg g^{-1}) represent the maximum adsorption uptake of the Langmuir equation, whilst K_L (L mg^{-1}) and K_F ((mg g^{-1}) (L mg^{-1})$^{1/n}$) are adjustable parameters of the two models, respectively; n is another adjustable parameter and is a measure of the adsorption heterogeneity.

3.5. Regeneration Process

The regeneration studies examined a simple procedure for both pollutants (Cipro and MB), as explained in the text.

3.6. Characterization of Samples

The nitrogen adsorption–desorption isotherm at 77 K was determined using a Quantachrome Quadrasorb equipped with a turbomolecular pump, after outgassing the samples for 8 h at 120 °C, using a heating rate of 1 °C min^{-1} to reach the final temperature. The BET area was obtained by the application of the Brunauer–Emmett–Teller (BET) method to the adsorption data using the criteria recommended by the IUPAC [16], while the pore size distribution was calculated based on non-local density functional theory (NLDFT) using the Quantachrome software ASiQwin version 3.01. The pattern of X-ray diffraction (XRD) was obtained using a Philips PW131 diffractometer (λ_{Cu} = 1.5454 Å). Dynamic light scattering (DLS) analysis was performed using a zeta sizer nano zs—Malvern to determine the Z average, size distribution, polydispersity and zeta potential of amorphous silica. Moreover, an infrared spectroscopy (FTIR) ATR spectrometer (Spectrum Two FT-IR Spectrometer, PerkinElmer) was employed to investigate the functional groups across a range of 4000 to 400 cm^{-1}, with a resolution of 4 cm^{-1} while SEM-EDX was used to determine the morphology and chemical composition. Thermal analyses (TGA and DSC) of AS-Si were realized from room temperature to 900 °C at a heating rate of 10 °C/min under air.

4. Conclusions

The underexploited region of the Moroccan oil shale was successfully converted into a valuable nanomaterial (silica) using the sol–gel process, which efficiently removes organic pollutants from the aqueous solution. The different analyses of XRD, FTIR, DLS, TGA, BET and NLDFT, DSC, and SEM-EDX confirm the amorphous structure of AS-Si with a moderate surface area and mesopore size, which are behind the efficient adsorption. The isotherm and kinetic studies of the two contaminants revealed a significant uptake capacity, most likely due to specific interactions with methylene blue and ciprofloxacin, including electrostatic attractions and hydrogen bonding.

The robust adsorption after four cycles noticed in this work makes the Rif region of MOSA useful as an alternative precursor for silica due to the low cost, eco-friendly nature, and abundance of this local resource, aligning with the sustainability goals, which highlights the importance of further research on this overlooked region.

In addition to the water treatment, the amorphous silica successfully extracted from the Moroccan oil shale ash in this work could also be useful in agroecological systems. A potentially interesting future application of the amorphous silica (AS-Si) is its use as a desiccant agent in integrated pest management systems, as many recent studies have indicated that silica-based formulations can act effectively against insects by promoting dehydration through disruption of the insect cuticle. This chemical-free approach represents a promising and sustainable strategy for agroecological applications. In addition, the physico-chemical properties of AS-Si, including its eco-friendliness, high purity, and surface area, make it meaningful to circular economy strategies and environmental sustainability objectives.

References

1. Hu, X.; Lu, Y.; Li, W.; Wang, L.; Huang, X.; Yang, D. Effect of Supercritical Water Temperature on Pyrolysis Characteristics of Oil Shales. *Energy Fuels* **2025**, *39*, 8482–8494. [CrossRef]

2. Zhai, Y.; Yang, T.; Liu, B.; Zhu, Y.; Wang, X. Enhancing Oil Shale Pyrolysis through Swelling Pretreatment: Mechanisms and Product Distribution. *Fuel* **2025**, *399*, 135637. [CrossRef]

3. Krime, A.; Saoiabi, S.; Berrahou, S.; Latifi, S.; El Hammari, L.; Saoiabi, A. Adsorption of Organic Pollutants Using Moroccan Oil Shales: Optimization of the Adsorption Process Using a Factorial Design. *NanoWorld J.* **2023**, *9*, S396–S400. [CrossRef]

4. Doumbouya, M.; Kacemi, K.E.; Kitane, S. Production of Portland Cement Using Moroccan Oil Shale and Comparative Study between Conventional Cement Plant and Cement Plant Using Oil Shale. *J. Chem. Soc. Pak.* **2012**, *34*, 885–889.

5. Alsafasfeh, A.; Alawabdeh, M.; Alfuqara, D.; Gougazeh, M.; Amaireh, M.N. Oil Shale Ash as a Substitutional Green Component in Cement Production. *Adv. Sci. Technol. Res. J.* **2022**, *16*, 157–162. [CrossRef] [PubMed]

6. Li, X.; Zhang, W.; Ma, H.; Yan, Y.; Zhang, Y.; Sun, R.; Wang, D. Enhancement Mechanism of Early Age Strength in Cement Paste Induced by Oil Shale Residue. *Constr. Build. Mater.* **2025**, *465*, 140277. [CrossRef]

7. Bai, S.; Chang, Z.; Ren, Z.; Zhao, Y.; Pang, L. Adsorption of Cd^{2+} Ions onto Zeolites Synthesized from a Mixture of Coal Fly Ash and Oil Shale Ash in Aqueous Media. *RSC Adv.* **2025**, *15*, 11293–11300. [CrossRef] [PubMed]

8. Gao, G.M.; Miao, L.N.; Ji, G.J.; Zou, H.F.; Gan, S.C. Preparation and Characterization of Silica Aerogels from Oil Shale Ash. *Mater. Lett.* **2009**, *63*, 2721–2724. [CrossRef]

9. Koreeda, H.; Ishijima, M.; Kajihara, K. Cosolvent-Free Sol–Gel Synthesis of Macroporous Silica Gels from Tetramethoxysilane–Tetraethoxysilane Mixtures. *J. Solgel Sci. Technol.* **2024**, *113*, 48–55. [CrossRef]

10. Navik, R.; Wang, E.; Ding, X.; Qiu, K.X.; Li, J. Atmospheric Carbon Dioxide Capture by Adsorption on Amine-Functionalized Silica Composites: A Review. *Environ. Chem. Lett.* **2024**, *22*, 1791–1830. [CrossRef]

11. Kim, J.S.; Woo, S.Y.; Lee, J.G.; Kim, Y.D. Effect of Adsorption Isotherm and Kinetics on the Performance of Silica Gel-Based Adsorption Desalination System with Heat and Mass Recovery. *Desalination* **2024**, *577*, 117375. [CrossRef]

12. Ciğeroğlu, Z.; El Messaoudi, N.; Şenol, Z.M.; Başkan, G.; Georgin, J.; Gubernat, S. Clay-Based Nanomaterials and Their Adsorptive Removal Efficiency for Dyes and Antibiotics: A Review. *Mater. Today Sustain.* **2024**, *26*, 100735. [CrossRef]

13. Bano, K.; Singh, P.P.; Kumar, S.; Saeed, S.M.; Aggarwal, S.; Kumar, R.; Kaushal, S. Construction of Honey Bee Hive-like CuO/PbO Heterojunction Photocatalysts with Enhanced Antibiotic and Dye Degradation Activity under Visible Light. *Environ. Sci.* **2024**, *10*, 1714–1725. [CrossRef]

14. Pan, Y.; Abazari, R.; Tahir, B.; Sanati, S.; Zheng, Y.; Tahir, M.; Gao, J. Iron-Based Metal–Organic Frameworks and Their Derived Materials for Photocatalytic and Photoelectrocatalytic Reactions. *Coord. Chem. Rev.* **2024**, *499*, 215538. [CrossRef]

15. Sing, K.S.W.; Everett, D.H.; Haul, R.A.W.; Moscou, L.; Pierotti, R.A.; Rouquerol, J.; Siemieniewska, T. Reporting Physisorption Data for Gas/Solid Systems with Special Reference to the Determination of Surface Area and Porosity. *Pure Appl. Chem.* **1985**, *57*, 603–619. [CrossRef]

16. Thommes, M.; Kaneko, K.; Neimark, A.V.; Olivier, J.P.; Rodriguez-Reinoso, F.; Rouquerol, J.; Sing, K.S.W. Physisorption of Gases, with Special Reference to the Evaluation of Surface Area and Pore Size Distribution (IUPAC Technical Report). *Pure Appl. Chem.* **2015**, *87*, 1051–1069. [CrossRef]

17. Negash, E.A.; Brehane Tesfamariam, B.; Mengesha, G.A.; Shasho, Y.; Mekuriya, Y.S.; Beyene, S.T. High-Purity Amorphous Silica from Industrial Filter Cake Waste: Synthesis and Process Optimization. *Mater. Res. Express* **2025**, *12*, 015201. [CrossRef]

18. Periakaruppan, R.; Chandrasekaran, N.; T, S.K.; Sasthri, G.; Al-Dayan, N. Green Synthesis of Silica Nanoparticles Using Enhalus Acoroides: Characterization and Antioxidant Activity. *Biomass Convers. Biorefin.* **2025**, 1–8. [CrossRef]

19. Zothansanga, C.; Dawngliana, K.M.S.; Zathang, B.; Rai, S. Investigation of Judd-Ofelt Parameters, Luminescent Properties and Energy Transfer Analysis of Eu3+ Doped Al in Silica Glass Matrix Synthesized via Sol-Gel Technique. *Opt. Mater.* **2025**, *159*, 116598. [CrossRef]

20. Jin, C.; Wang, J.; Wang, Y.; Tang, H.; Lu, T. Fabrication of Hierarchically Porous Silica Nanospheres through Sol-Gel Process and Pseudomorphic Transformation. *J. Solgel Sci. Technol.* **2014**, *70*, 53–61. [CrossRef]

21. Santos, G.M.; Leong, C.A.; Grootes, P.M.; Seiler, M.; Svarva, H.; Nadeau, M.J. Radiocarbon Step-combustion Oxidation Method and Ftir Analysis of Trondheim $CaCO_3$ Precipitates of Atmospheric CO_2 samples: Further investigations and insights. *Radiocarbon* **2024**, *66*, 1289–1301. [CrossRef]

22. Leventaki, E.; Baena-Moreno, F.M.; Sardina, G.; Ström, H.; Ghahramani, E.; Naserifar, S.; Ho, P.H.; Kozlowski, A.M.; Bernin, D. In-Line Monitoring of Carbon Dioxide Capture with Sodium Hydroxide in a Customized 3D-Printed Reactor without Forced Mixing. *Sustainability* **2022**, *14*, 10795. [CrossRef]

23. Krime, A.; Eloufir, M.R.; Saoiabi, S.; Tlemcani, M.; Morais, M.; Saoiabi, A. Extracting High Purity Nano-Silica from Oil Shale: Valorising a Neglected Natural Resource. *Mater. Res. Bull.* **2025**, *192*, 113561. [CrossRef]

24. Gorbunova, O.V.; Baklanova, O.N.; Gulyaeva, T.I.; Trenikhin, M.V.; Drozdov, V.A. Poly(Ethylene Glycol) as Structure Directing Agent in Sol–Gel Synthesis of Amorphous Silica. *Microporous Mesoporous Mater.* **2014**, *190*, 146–151. [CrossRef]

25. Hatem, R.S.; Hussain, A.F.; Mihsen, H.H. Green Synthesis, Characterization, and Adsorption of Co(II) and Cu(II) Ions from Aqueous Solution by Mesoporous Silica MCM-41. *Chem. Pap.* **2024**, *78*, 6331–6342. [CrossRef]

26. Sawangprom, A.; Jampreecha, T.; Maensiri, S. Synthesis and Characterization of High-Purity SiO_2 Nanoparticles Utilizing Greater Club Rush: Exploring a Promising Natural Source. *Int. J. Miner. Metall. Mater.* **2025**, *32*, 1234–1244. [CrossRef]

27. Guo, S.; Ali, M.A.; Mohamed, M.A.; Han, X.; Liu, X.; Qiu, J. Reduction of Injection Molded Silica Glass Defects and Enhancement of Glass Quality via Water Debinding. *Mater. Chem. Front.* **2024**, *8*, 1400–1408. [CrossRef]

28. Li, Y.; Zhang, H.; Chen, J.; Xiang, T.; Cheng, Y.; Zhang, H. Effect of Hydrophobic Fumed Silica on Bending Strength of Sodium Silicate-Bonded Sand Cores. *Materials* **2024**, *17*, 5714. [CrossRef] [PubMed]

29. Giovannini, G.; Kunc, F.; Piras, C.C.; Stranik, O.; Edwards, A.A.; Hall, A.J.; Gubala, V. Stabilizing Silica Nanoparticles in Hydrogels: Impact on Storage and Polydispersity. *RSC Adv.* **2017**, *7*, 19924–19933. [CrossRef]

30. Breznan, D.; Nazemof, N.; Kunc, F.; Hill, M.; Vladisavljevic, D.; Gomes, J.; Johnston, L.J.; Vincent, R.; Kumarathasan, P. Acellular Oxidative Potential Assay for Screening of Amorphous Silica Nanoparticles. *Analyst* **2020**, *145*, 4867–4879. [CrossRef] [PubMed]

31. Kanwal, A.; Abid, J.; Waqar-Un-Nisa; Gul, S.; Nouman, M.; Idris, A.M.; Ullah, H. Nickel-Modified Orange Peel Biochar for the Efficient Adsorptive Removal of Eriochrome Black T from Aqueous Solution. *Water* **2025**, *17*, 1484. [CrossRef]

32. Vinu, A.A.; Murugesan, V.; Tangermann, O.; Hartmann, M. Adsorption of Cytochrome c on Mesoporous Molecular Sieves: Influence of pH, Pore Diameter, and Aluminum Incorporation. *Chem. Mater.* **2004**, *16*, 3056–3065. [CrossRef]

33. Hemdan, S.S. The Shift in the Behavior of Methylene Blue Toward the Sensitivity of Medium: Solvatochromism, Solvent Parameters, Regression Analysis and Investigation of Cosolvent on the Acidity Constants. *J. Fluoresc.* **2023**, *33*, 2489–2502. [CrossRef] [PubMed]

34. Igwegbe, C.A.; Oba, S.N.; Aniagor, C.O.; Adeniyi, A.G.; Ighalo, J.O. Adsorption of Ciprofloxacin from Water: A Comprehensive Review. *J. Ind. Eng. Chem.* **2021**, *93*, 57–77. [CrossRef]

35. Al-Qodah, Z.; Lafi, W.K.; Al-Anber, Z.; Al-Shannag, M.; Harahsheh, A. Adsorption of Methylene Blue by Acid and Heat Treated Diatomaceous Silica. *Desalination* **2007**, *217*, 212–224. [CrossRef]

36. Macena, M.; Pereira, H.; Cruz-Lopes, L.; Grosche, L.; Esteves, B. Competitive Adsorption of Metal Ions by Lignocellulosic Materials: A Review of Applications, Mechanisms and Influencing Factors. *Separations* **2025**, *12*, 70. [CrossRef]

37. Daizy, M.; Ali, M.R.; Bacchu, M.S.; Aly, M.A.S.; Khan, M.Z.H. ZnO Hollow Spheres Arrayed Molecularly-Printed-Polymer Based Selective Electrochemical Sensor for Methyl-Parathion Pesticide Detection. *Environ. Technol. Innov.* **2021**, *24*, 101847. [CrossRef]

38. Yuan, N.; Cai, H.; Liu, T.; Huang, Q.; Zhang, X. Adsorptive Removal of Methylene Blue from Aqueous Solution Using Coal Fly Ash-Derived Mesoporous Silica Material. *Adsorpt. Sci. Technol.* **2019**, *37*, 333–348. [CrossRef]

39. Kumar, K.V.; Ramamurthi, V.; Sivanesan, S. Modeling the Mechanism Involved during the Sorption of Methylene Blue onto Fly Ash. *J. Colloid. Interface Sci.* **2005**, *284*, 14–21. [CrossRef] [PubMed]

40. Bhattacharya, K.G.; Sharma, A. Kinetics and Thermodynamics of Methylene Blue Adsorption on Neem (*Azadirachta indica*) Leaf Powder. *Dye. Pigment.* **2005**, *65*, 51–59. [CrossRef]

41. Hongo, T.; Moriura, M.; Hatada, Y.; Abiko, H. Simultaneous Methylene Blue Adsorption and PH Neutralization of Contaminated Water by Rice Husk Ash. *ACS Omega* **2021**, *6*, 21604–21612. [CrossRef] [PubMed]

42. Liu, T.; Liu, W.; Li, X.; Wang, H.; Lan, Y.; Zhang, S.; Wang, Y.; Liu, H. Effect of Environmental Factors on Adsorption of Ciprofloxacin from Wastewater by Microwave Alkali Modified Fly Ash. *Sci. Rep.* **2024**, *14*, 19831. [CrossRef] [PubMed]

43. Hussain, Z.; Ali, G.; Akbar, A.R.; Khan, K.U.; Al-Khattaf, F.S.; Saleem, A. Physicochemical Synthesis of Zeolite Modified Nano-Flakes to Eliminate Emerging Pollutants in Aquatic Environment. *J. Water Process Eng.* **2025**, *69*, 106832. [CrossRef]

44. Moreira, C.A.; Scanferla, C.E.; Oliveira, A.G.; Duarte, V.A.; Arroyo, P.A.; de Lara Andrade, J.; Bittencourt, P.R.S.; Garcia, J.C.; de Oliveira, D.M.F. Bio-Adsorbents Based on Mesoporous Silica Produced from Rice Husks with Tunable Architecture and Surface Area for Remediation of Industrial Effluents. *J. Porous Mater.* **2024**, *32*, 27–46. [CrossRef]

45. Lu, D.; Xu, S.; Qiu, W.; Sun, Y.; Liu, X.; Yang, J.; Ma, J. Adsorption and Desorption Behaviors of Antibiotic Ciprofloxacin on Functionalized Spherical MCM-41 for Water Treatment. *J. Clean. Prod.* **2020**, *264*, 121644. [CrossRef]

46. Li, P.; Zhao, L.; Li, L.; Xu, K.; Iqbal, J.; Tian, Z.; Xing, X.; Li, H.; Hou, Y.; Wang, J.; et al. Preparation of Mg-Doped Coffee Waste for Efficient Removal of Methylene Blue and Lead from Water. *Heliyon* **2025**, *11*, e43091. [CrossRef]

47. Mujiyanti, D.R.; Santoso, U.T.; Saptarini, M.D.; Emi, N.H. Synthesis and Characterization Nanosilica from Rice Husk Ash Using Sol-Gel Method with Addition of PEG-6000 and PVA. *JKPK (J. Kim. Dan Pendidik. Kim.)* **2021**, *6*, 252–263. [CrossRef]

48. Jabłońska, B.; Jabłoński, P.; Gęga, J. Kinetics and Thermodynamics of Pb(II), Zn(II), and Cd(II) Adsorption from Aqueous Solutions onto Activated Biochar Obtained from Tobacco Waste. *Materials* **2025**, *18*, 2324. [CrossRef] [PubMed]

49. Haoufazane, C.; Zaaboul, F.; El Monfalouti, H.; Sebbar, N.K.; Hefnawy, M.; El Hourch, A.; Kartah, B.E. A Sustainable Solution for the Adsorption of C.I. Direct Black 80, an Azoic Textile Dye with Plant Stems: Zygophyllum Gaetulum in an Aqueous Solution. *Molecules* **2024**, *29*, 4806. [CrossRef] [PubMed]

50. Zaaboul, F.; Kaichouh, G.; Haoufazane, C.; Abuelizz, H.A.; Karrouchi, K.; Zarrouk, A.; El Hourch, A. Adsorption of Reactive Blue Day 49 from Aqueous Solution on Commercial Activated Carbon and Polyaniline Electrochemically Deposited on Carbon Felt: Kinetic Modeling and Equilibrium Isotherm Analysis. *Int. J. Electrochem. Sci.* **2024**, *19*, 100713. [CrossRef]

51. Benazouz, K.; Bouchelkia, N.; Moussa, H.; Boutheldja, R.; Zamouche, M.; Amrane, A.; Parvathiraja, C.; Al-Lohedan, H.A.; Bollinger, J.C.; Mouni, L. Efficient Removal of Cu(II) from Wastewater Using Chitosan Derived from Shrimp Shells: A Kinetic, Thermodynamic, Optimization, and Modelling Study. *Water* **2025**, *17*, 851. [CrossRef]

52. Karleuša, R.; Marinić, J.; Tomić Linšak, D.; Dubrović, I.; Antunović, D.; Broznić, D. The Hidden Legacy of Dimethoate: Clay Binding Effects on Decreasing Long-Term Retention and Reducing Environmental Stability in Croatian Soils. *Toxics* **2025**, *13*, 219. [CrossRef] [PubMed]